Probability distributions in classical and quantum elliptic billiards

Julio C. Gutiérrez-Vega and Sabino Chávez-Cerda
Grupo de Fotónica y Física Óptica, Instituto Nacional de Óptica y Electrónica
Apartado postal 51 y 216, 72000 Puebla, Pue., Mexico

Ramón M. Rodríguez-Dagnino
Centro de Electrónica y Telecomunicaciones, Instituto Tecnológico y de Estudios Superior de Monterrey
Garza Sada 2501, Col. Tecnológico, Monterrey, N.L., Mexico

Recibido el 17 de mayo de 2001; aceptado el 14 de agosto de 2001

Advances in the fabrication of nanocavities to confine electrons have popularized newly the study of 2D quantum wells. The analogies and differences between classical and quantum probability distributions and energy spectra of a particle confined in an elliptic billiard are presented. Classically, the probability densities are characterized by the eigenvalues of an equation that involves elliptic integrals, whereas the ordinary and modified Mathieu functions are applied to describe the quantum distributions. The transition from the elliptic geometry toward the circular geometry is analyzed as well. The problem is interesting itself because it presents strong analogies with the electromagnetic propagation in elliptic waveguides.

Keywords: Quantum and classical elliptic billiard; Mathieu functions; Hamilton-Jacobi theory; elliptic integrals

Los avances en la fabricación de nanocavidades para confinar electrones han popularizado nuevamente el estudio de pozos cuánticos bidimensionales. En este trabajo se presentan las analogías y diferencias entre las distribuciones de probabilidad y espectros de energía de una partícula confinada en un billar elíptico. Clásicamente las densidades de probabilidad están caracterizadas por los eigenvalores de una ecuación que involucra integrales elípticas, mientras las ecuaciones radial y angular de Mathieu se aplican para describir las distribuciones cuánticas. La transición de la geometría elíptica a circular es analizada también. El problema es interesante pues presenta muchas analogías con la propagación electromagnética en guías de onda elípticas.

Descriptores: Billar elíptico clásico y cuántico; funciones de Mathieu; teoría de Hamilton-Jacobi; integrales elípticas

PACS: 02.30.-f; 02.30.Jr

1. Introduction

The study of energy spectra of physical systems plays a fundamental role in quantum mechanics (QM). The problem of a free particle moving in an one-dimensional (1D) infinite well may be the first and most frequently solved eigenvalue problem in elementary QM textbooks [1, 2]. The simplicity of the 1D model permits us to get a first insight about important results of QM (*e.g.*, normalized wave functions, energy-level spacings). Usually, the two-dimensional (2D) infinite rectangular billiard is considered to show the existence of degeneracies [2], and infinite circular billiard is useful to introduce the concept of angular momentum [3] and also presents degeneracies. Evidently most of the textbooks are focused to study the quantum phenomena involving three-dimensional systems (*e.g.*, probability distributions in an atom of hydrogen).

The 2D systems have became more popular in recent years because progress in nanotechnology have allowed to fabricate very small closed structures (*i.e.*, quantum corrals), which can be used to confine electrons [4]. The boundary of the nanodevices is sharp enough to consider that the electron may be regarded as a particle confined to a 2D infinite billiard. Hence the energy spectrum of the electron can be described by solving the appropriate Schrödinger wave equation inside the billiard with the Dirichlet condition at the boundary. In addition, the study of trajectories in 2D billiards is of particular interest in classical and quantum chaos as well [5].

As we mentioned above, the rectangular and circular billiards are well-treated in textbooks, however we think that this is not the case with the elliptic geometry. Due to the renewed attention in 2D systems, the purpose of our work is to present a study of the classical and quantum elliptic billiard as an example of a 2D system with non-degenerate states. Besides, the quantum elliptic billiard has exact analytical solutions which allow us to write the eigenfunctions in a closed form, namely Mathieu functions. In order to establish a connection between classical and quantum mechanics, we compare the probability distributions to show that both approach each other as the energy increases. Our results are compared with respect to known literature of elliptic billiards (see Refs. 6–9, and 11, and references therein).

This work is intended also for researchers who are interested in the solution of the Schrödinger equation in elliptic coordinates and the application of Mathieu functions. In such a way, this paper may be considered as a continuation of one preceding [10], where we discuss the free oscillations of an elliptic membrane, and include a more detailed treatment of the Mathieu function theory. Part of the results included in this paper were already discussed in Ref. 11. On the other hand, the problem may result interesting to researchers involved in the study of propagation of light inside elliptic waveguides, due to the strong analogies between classical mechanics solutions with the ray-trajectories in geometrical optics, and the QM solutions with the propagating modes in electromagnetic theory.

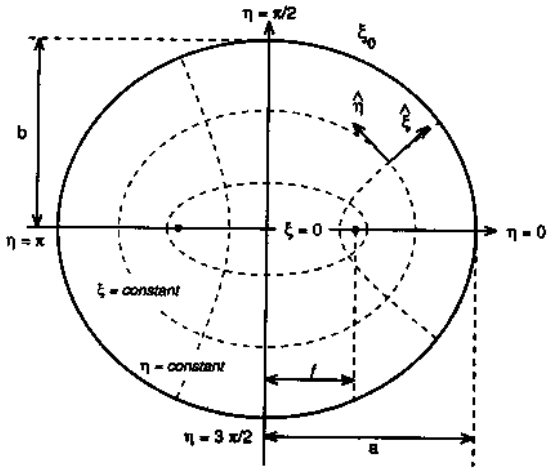

FIGURE 1. Geometry of the billiard in elliptic coordinates. The boundary is given by $\xi = \xi_0$ and the range of the coordinates are $\xi \in [0, \infty)$ and $\eta = [0, 2\pi)$.

The paper is organized as follows. In Sec. 2, we present the procedure to obtain the classical trajectories for periodic orbits in the billiard. The eigenfunctions corresponding to quantum billiard are given in Sec. 3. The probability distributions for classical and quantum cases are compared in Sec. 4, where the energy spectrum for elliptic billiard is compared with respect to circular billiard also. Finally, in the conclusions we point out some final comments.

2. Classical mechanics solution

The geometry of the elliptic billiard is shown in Fig. 1. Classically speaking, the particle moves freely inside the billiard and it is elastically bounced at the boundary. The system presents two degrees of freedom and two constants of motion [12], the first of them is the total energy E and the second one is the dot product of the angular momenta with respect to the foci of the ellipse, $\Lambda = \mathbf{L}_1 \cdot \mathbf{L}_2$. It follows that elliptic billiard is an *integrable system* whose dynamical behavior is regular and predictable. In general, the motion of the particle is characterized in terms of the canonical coordinates q_i and canonical momenta p_i. Because there exist two constants of motion, the particle is restricted to move in a specific trajectory in the phase space (q_i, p_i), where E and Λ are maintained fixed.

In particular, we are interested in periodic trajectories in the billiard. An effective method of handling these periodic systems is provided by the application of *action-angle variables* in the Hamilton-Jacobi theory (HJT). In HJT terminology, the constants of motion are called the *action variables* of the system and they are often represented as $J_i(q_i, p_i)$. For each $J_i(q_i, p_i)$ there exist a corresponding *angle variable* designated by $\Theta_i(q_i, p_i)$. The action variable J_i is determined by

$$J_i = \frac{1}{2\pi} \oint p_i \, dq_i, \tag{1}$$

where the contour integral is carried out over a complete period of the coordinate q_i. The angle variable Θ_i corresponds to the frequency ω_i of the periodic motion of the coordinate q_i and is given by

$$\omega_i \equiv \frac{d\Theta_i}{dt} = \frac{\partial H(J, \Theta)}{\partial J_i}, \tag{2}$$

where H is the hamiltonian of the system. In our two-dimensional billiard, the periodic trajectories are determined by the condition that ω_1/ω_2 must be equal to r/n. A detailed treatment of Hamilton-Jacobi theory can be found in Ref. 13.

Let us first introduce the elliptic coordinates

$$x = f \cosh\xi \cos\eta, \qquad y = f \sinh\xi \sin\eta.$$

The boundary of the elliptic billiard is expressed as $\xi = \xi_0 = \operatorname{arctanh}(b/a) = \text{constant}$, where a and b are the semi-major axis and semi-minor axis of the ellipse, respectively, $(b < a)$. The semifocal distance f is given by $f^2 = a^2 - b^2$, and the eccentricity e is defined as

$$e = \frac{f}{a} = \frac{1}{\cosh\xi_0}. \tag{3}$$

The velocity of the particle as a function of the elliptic coordinates is

$$\mathbf{v} = h_1 \frac{d\xi}{dt}\hat{\boldsymbol{\xi}} + h_2 \frac{d\eta}{dt}\hat{\boldsymbol{\eta}}, \tag{4}$$

where h_1 and h_2 are the metric factors of the generalized coordinates $q_1 = \xi$ and $q_2 = \eta$ given by

$$h_1^2 = h_2^2 = h^2 = \frac{f^2}{2}(\cosh 2\xi - \cos 2\eta), \tag{5}$$

and $\hat{\boldsymbol{\xi}}$ and $\hat{\boldsymbol{\eta}}$ are the elliptic unit vectors related to cartesian unit vectors by

$$\begin{pmatrix} \hat{x} \\ \hat{y} \end{pmatrix} = \frac{f}{h} \begin{pmatrix} \sinh\xi\cos\eta & -\cosh\xi\sin\eta \\ \cosh\xi\sin\eta & \sinh\xi\cos\eta \end{pmatrix} \begin{pmatrix} \hat{\boldsymbol{\xi}} \\ \hat{\boldsymbol{\eta}} \end{pmatrix}. \tag{6}$$

According to classical mechanics theory, the canonical momenta are expressed as

$$p_\xi = \frac{\partial L}{\partial \dot{\xi}} = Mh^2 \frac{d\xi}{dt},$$
$$p_\eta = \frac{\partial L}{\partial \dot{\eta}} = Mh^2 \frac{d\eta}{dt}, \tag{7}$$

where $L = (1/2)Mh^2\left[(d\xi/dt)^2 + (d\eta/dt)^2\right]$ is the lagrangian and M is the mass of the particle. For our conservative billiard, the hamiltonian is equal to the total mechanical energy E, and it can be written in terms of canonical momenta as

$$H = E = \frac{p_\xi^2 + p_\eta^2}{2Mh^2}. \tag{8}$$

As we mentioned previously, the second constant of motion is the product of angular momenta with respect to the foci

$$\Lambda = \mathbf{L}_1 \cdot \mathbf{L}_2 = (\mathbf{r}_1 \times M\mathbf{v}) \cdot (\mathbf{r}_2 \times M\mathbf{v}),$$

where $\mathbf{r}_1 = (x-f)\hat{\boldsymbol{x}} + y\hat{\boldsymbol{y}}$ and $\mathbf{r}_2 = (x+f)\hat{\boldsymbol{x}} + y\hat{\boldsymbol{y}}$. By using Eqs. (4) and (6), we can obtain Λ as a function of the elliptical coordinates

$$\Lambda = M^2 f^2 h^2 \left[\left(\frac{d\eta}{dt}\right)^2 \sinh^2\xi - \left(\frac{d\xi}{dt}\right)^2 \sin^2\eta \right],$$

which can also be expressed as a function of the canonical momenta by Eq. (7)

$$\Lambda = \frac{f^2}{h^2}\left(p_\eta^2 \sinh^2\xi - p_\xi^2 \sin^2\eta\right). \tag{9}$$

The conserved quantity Λ is a useful parameter to define the kind of motion of the particle. In general, there are two types of motion depending on the sign of Λ. The first case, $\Lambda > 0$, corresponds to trajectories that have an inner elliptic caustic $\xi = \xi_c = \text{constant} > 0$, confocal to the boundary and, therefore, the particle never crosses the x-axis between the foci. In this case, the ξ coordinate is restricted to oscillate in the range $\xi \in [\xi_c, \xi_0]$ whereas the η coordinate does not have any restrictions. We will identify this motion as *rotational type* (R), (see Fig. 3).

On the other hand, in the second type of motion, $\Lambda < 0$, the trajectories generate two caustics in the form of cofocal hyperbolas, $\eta = \eta_c$ and $\eta = \pi - \eta_c$, where $\eta_c < \pi/2$. Now, the particle always cross the x-axis between the foci and the bounces happen alternately in the upper and lower parts of the billiard. The η coordinate of the particle is limited to vibrate in the range $\eta \in [\eta_c, \pi - \eta_c]$, whereas the ξ coordinate oscillates in the whole range $\xi \in [0, \xi_0]$. As above, we will identify this motion as *oscillating type* O, (see Fig. 5).

The separatrix occurs when $\Lambda = 0$, and the particle just crosses over the focal points. It should be mentioned that the range of Λ is limited to

$$\Lambda \in \left[-2MEf^2, 2MEb^2\right],$$

where the lower limit $\Lambda_{\min} = -2MEf^2$ corresponds to the motion along the y-axis and the upper limit $\Lambda_{\max} = 2MEb^2$ represents the limiting motion over the boundary. Because Λ is energy-dependent, it is preferable to define a new energy-independent parameter, say γ, given by

$$\gamma = \frac{\Lambda}{2MEf^2} \in \left[-1, \left(\frac{b}{f}\right)^2\right]. \tag{10}$$

In terms of γ, the eccentricity of the caustic e_c is determined by

$$e_c = \frac{f}{a_c} = \frac{1}{\sqrt{1+\gamma}}. \tag{11}$$

The canonical momenta Eq. (7) can be written as a function of γ and E as follows

$$p_\xi^2 = 2MEf^2\left(\sinh^2\xi - \gamma\right),$$
$$p_\eta^2 = 2MEf^2\left(\sin^2\eta + \gamma\right).$$

By inserting the momenta $p_\xi(E,\gamma)$ and $p_\eta(E,\gamma)$ in Eq. (1), the actions are given by

$$J_\xi = 2\sqrt{\frac{MEf^2}{2\pi^2}} \int_{\xi_c}^{\xi_0} \sqrt{\sinh^2\xi - \gamma}\, d\xi, \tag{12}$$

$$J_\eta = 4\sqrt{\frac{MEf^2}{2\pi^2}} \int_{\eta_c}^{\pi/2} \sqrt{\sin^2\eta + \gamma}\, d\eta, \tag{13}$$

where the lower limits of the integrals are different depending on the kind of motion. For rotational motion ($\gamma > 0$), $\xi_c = \operatorname{arccosh}(1/e_c)$ and $\eta_c = 0$. For oscillating motion ($\gamma < 0$), $\xi_c = 0$ and $\eta_{\min} = \arccos(1/e_c)$.

The condition of periodic trajectories is reached when the quotient of the frequencies associated to each coordinate is a rational number. According to Eq. (2), we have

$$\frac{\omega_\xi}{\omega_\eta} = \frac{\dfrac{\partial H}{\partial J_\xi}}{\dfrac{\partial H}{\partial J_\eta}} = \frac{\partial J_\eta}{\partial J_\xi} = \frac{\left|\dfrac{\partial J_\eta}{\partial \gamma}\right|}{\left|\dfrac{\partial J_\xi}{\partial \gamma}\right|} = \frac{r}{n}. \tag{14}$$

By differentiating Eqs. (12) and (13) with respect to γ, and after some manipulations, we arrive to

$$\frac{\partial J_\xi}{\partial \gamma} = \begin{cases} -\sqrt{\dfrac{ME}{2\pi^2}}\,\dfrac{e_c}{f}\,F(\phi_1, e_c^2), & \gamma > 0, \\ -\sqrt{\dfrac{ME}{2\pi^2}}\,\dfrac{1}{f}\,F\left(\phi_2, \dfrac{1}{e_c^2}\right), & \gamma < 0, \end{cases} \tag{15}$$

$$\frac{\partial J_\eta}{\partial \gamma} = \begin{cases} \dfrac{\sqrt{2ME}}{\pi}\,\dfrac{e_c}{f}\,F\left(\dfrac{\pi}{2}, e_c^2\right), & \gamma > 0, \\ \dfrac{\sqrt{2ME}}{\pi}\,\dfrac{1}{f}\,F\left(\dfrac{\pi}{2}, \dfrac{1}{e_c^2}\right), & \gamma < 0, \end{cases} \tag{16}$$

where $\sin\phi_1 = \sqrt{1 - (f^2/b^2)\gamma}$, $\sin\phi_2 = \sqrt{b^2/(b^2 - f^2\gamma)}$, and $F(\theta, m)$ is the elliptic integral of the first kind [14], given by

$$F(\theta, m) = \int_0^\theta \frac{d\theta}{\sqrt{1 - m\sin^2\theta}}.$$

Finally, by substituting Eqs. (15) and (16) in Eq. (14), the characteristic equations for periodic trajectories are

$$F\left(\frac{\pi}{2}, e_c^2\right) = \frac{r}{2n} F(\phi_1, e_c^2), \qquad \gamma > 0, \tag{17}$$

$$F\left(\frac{\pi}{2}, \frac{1}{e_c^2}\right) = \frac{r}{2n} F\left(\phi_2, \frac{1}{e_c^2}\right), \qquad \gamma < 0. \tag{18}$$

The roots of the characteristic equations are the possible values of γ to have periodic orbits in the billiard.

2.1. Periodic trajectories

We first discuss the rotational trajectories characterized by Eq. (17). By applying the jacobian elliptic function $sn(u)$ to

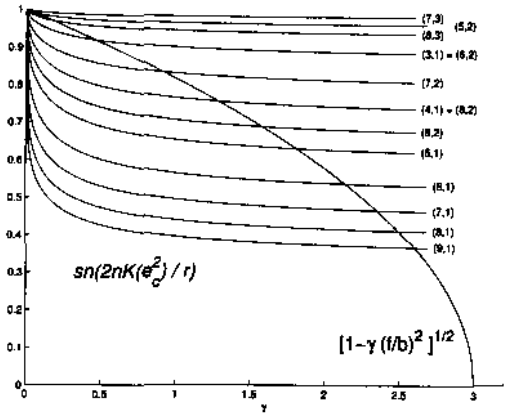

FIGURE 2. Plots of characteristic equation for R-trajectories for an ellipse with $b/a = \sin(\pi/3)$ and $f = 0.5$.

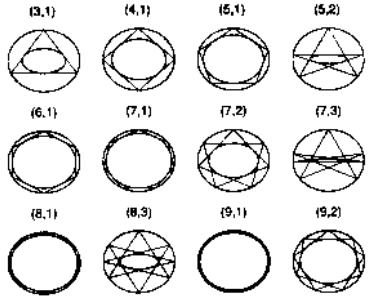

FIGURE 3. Periodic R-trajectories corresponding to data in Fig. 2.

both sides of the Eq. (17), we can obtain

$$\sqrt{1-\left(\frac{f^2}{b^2}\right)\gamma} = sn\left[\frac{2n}{r}K\left(e_c^2\right)\right], \qquad \gamma > 0, \qquad (19)$$

where $K(m) = F(\pi/2, m)$ is the complete elliptic integral of the first kind. Equation (19) has real solutions for $r \geq 3$ and $n < r/2$. The parameters r and n are the number of bounces at the boundary and the rotation number respectively. In Fig. 2 we plot both sides of the Eq. (19) for the first values of r and n. The intersections correspond to the eigenvalues of γ to have closed trajectories inside the billiard. The paths associated to the eigenvalues of γ are plotted in Fig. 3. We should mention that we have taken advantage of MATLAB software utilities [15] to implement all plots in this work.

On the other hand, Eq. (18) is inverted as follows

$$\sqrt{\frac{b^2}{b^2 - f^2\gamma}} = sn\left[\frac{2n}{r}K\left(\frac{1}{e_c^2}\right)\right], \qquad \gamma < 0. \qquad (20)$$

The above equation has real solutions for $r \geq 4$ and $n < r/2$, where r must be an even integer in order to have closed oscillating trajectories. Furthermore, a certain O-trajectory (r, n) can be present in the ellipse only if it satisfies the next cut-off condition

$$\sin\frac{n}{r}\pi \geq \frac{b}{a},$$

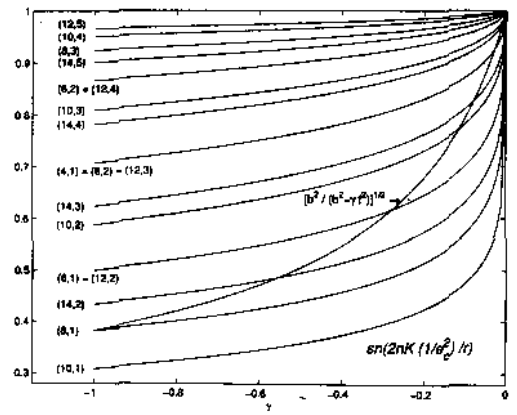

FIGURE 4. Plots of the characteristic equation for O-trajectories for an ellipse with $b/a = \sin(\pi/8)$. The curve $(8, 1)$ corresponds to cut-off condition $n/r = 1/8$ and, therefore, intersect at limit $\gamma = -1$. Observe that curve $(10, 1)$ does not intersect because it is out of the valid range $1/8 \leq n/r < 1/2$.

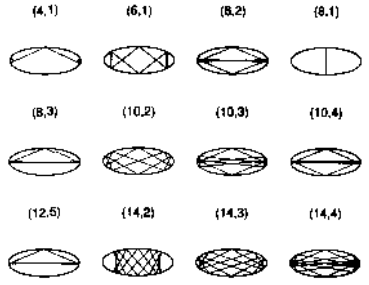

FIGURE 5. Periodic O-trajectories corresponding to data in Fig. 4.

where the equality corresponds to motion along the minor-axis of the ellipse as it is shown in Fig. 5. Both sides of the characteristic equation [Eq. (20)] are plotted in Fig. 4, where we have chosen $a = \sqrt{\sin(\pi/3)/\sin(\pi/8)}$ and $b/a = \sin(\pi/8)$, [*i.e.*, $e = \cos(\pi/8)$] with two purposes:

a) To match the trajectory $(8, 1)$ with the cut-off condition in order to visualize this situation.
b) To maintain the same area of the ellipse (πab) from the above rotating case (Fig. 2) in order to make appropriate comparisons with the quantum solutions.

3. Quantum mechanics solution

The quantum energy spectrum of a particle in the infinite billiard is obtained by solving the time-independent Schrödinger equation

$$\hat{H}\varphi(\xi,\eta) \equiv \left[-\frac{\hbar^2}{2M}\nabla^2 + U(\xi,\eta)\right]\varphi(\xi,\eta) = E\varphi(\xi,\eta), \quad (21)$$

where $\hat{H}$ is the energy operator (*i.e.* the hamiltonian), $\varphi(\xi, \eta)$ is the eigenfunction corresponding to the characteristic energy E, and $U(\xi, \eta)$ is the potential energy expressed by

$$U(\xi,\eta) = \begin{cases} 0, & \text{for } \xi \leq \xi_0, \\ \infty, & \text{for } \xi > \xi_0. \end{cases}$$

The eigenfunctions $\varphi(\xi,\eta)$ must satisfy the Dirichlet boundary condition $\varphi(\xi_0,\eta)=0$, and the periodicity condition $\varphi(\xi,\eta)=\varphi(\xi,\eta+2\pi)$. The laplacian operator expressed in elliptic coordinates is written as [10]

$$\nabla^2=\frac{1}{h^2}\frac{\partial^2}{\partial\xi^2}+\frac{1}{h^2}\frac{\partial^2}{\partial\eta^2}, \tag{22}$$

where h is given by Ec. (5). By replacing the laplacian in Eq. (21), and taking the fact that $U(\xi,\eta)=0$ in the billiard, the 2D Schrödinger equation (2D SE) in elliptical coordinates is written as follows

$$\left[\frac{\partial^2}{\partial\xi^2}+\frac{\partial^2}{\partial\eta^2}+\frac{k^2f^2}{2}(\cosh 2\xi-\cos 2\eta)\right]\varphi(\xi,\eta)=0,$$

where $k^2=2ME/\hbar^2$.

Supposing the solution $\varphi(\xi,\eta)=R(\xi)\Theta(\eta)$, the 2D SE is separated into the next two ordinary differential equations

$$R''(\xi)-(\alpha-2q\cosh 2\xi)R(\xi)=0, \tag{23}$$

$$\Theta''(\eta)+(\alpha-2q\cos 2\eta)\Theta(\eta)=0, \tag{24}$$

where α is the constant of separation and q is a dimensionless parameter given by

$$q=\frac{k^2f^2}{4}=\frac{Mf^2}{2\hbar^2}E. \tag{25}$$

The Eqs. (23) and (24) are known as modified Mathieu equation (MME) and ordinary Mathieu equation (OME), respectively. The solutions to these Equations are known as modified Mathieu functions (MMF) and ordinary Mathieu functions (OMF) [16], respectively.

We first consider the solution of OME [Eq. (24)]. Since the OMF must be periodic, we can express them in term of Fourier series

$$\Theta_r(\eta)=\begin{cases} ce_r(\eta,q)=\sum_{k=0}^{\infty}A_k(r,q)\cos k\eta, \\ se_{r+1}(\eta,q)=\sum_{k=1}^{\infty}B_k(r,q)\sin k\eta, \end{cases} \tag{26}$$

where the order ($r\geq 0$) is related to the r-th eigenvalue α_r of the equation and $ce_r(\eta,q)$ and $se_{r+1}(\eta,q)$ are known as the even and odd Mathieu functions, respectively. These eigenvalues are those values of α which, for a certain fixed parameter q, the OME admits solutions with period π or 2π.

For simplicity, we denote the eigenvalues associated to $ce_r(\eta,q_r)$ and $se_{r+1}(\eta,q_r)$ as $\alpha_r(q)$ and $\beta_{r+1}(q)$, respectively. According to the Sturm-Liouville theory, all eigenvalues are real and $\alpha_0<\beta_1<\alpha_1<\beta_2\ldots$ The plots of $\alpha_r(q)$ and $\beta_{r+1}(q)$ in the (q,α)-plane are lines that do not intersect (Fig. 6). The even-order solutions have period π, whereas odd-order solutions have period 2π. The Fourier coefficients $A_k(r,q_r)$ and $B_k(r,q_r)$ can be computed by using the well-known recurrence relations for the Mathieu equations [10, 14].

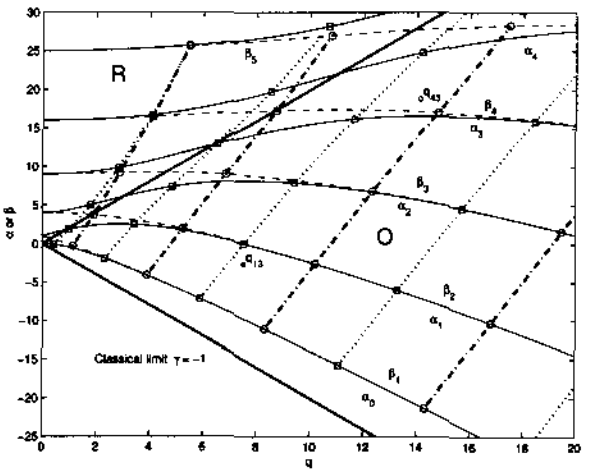

FIGURE 6. Plots of $\alpha_r(q)$ (solid curves), $\beta_{r+1}(q)$ (dashed curves), ${}_eq_m(\alpha)$ (dotted curves) and ${}_oq_m(\beta)$ (dash-dot curves) in the (q,α)-plane. The square markers correspond to ${}_eq_{r,m}$ eigenvalues (cross-points between α_r and ${}_eq_m$) and circle markers correspond to ${}_oq_{r,m}$ eigenvalues (cross-points between β_r and ${}_oq_m$) for an ellipse with data as in Fig. 2, (*i.e.*, $e=0.5$). We can appreciate that $\beta_r(q)\to\alpha_r(q)\to r^2$ as $q\to 0$ and that $\beta_{r+1}(q)\to\alpha_r(q)$ as $q\to\infty$.

On the other hand, the solutions for MME [Eq. (23)] is obtained from the OMF by setting the change of variable $\eta=i\xi$

$$R_r(\xi)=\begin{cases} Ce_r(\xi,q_r)=\sum_{k=0}^{\infty}A_k(r,q_r)\cosh k\xi, \\ Se_{r+1}(\xi,q_r)=\sum_{k=1}^{\infty}B_k(r,q_r)\sinh k\xi. \end{cases} \tag{27}$$

The Dirichlet condition at the boundary is satisfied when

$$R_r(\xi_0)=\begin{cases} Ce_r(\xi_0,q)=0, \\ Se_{r+1}(\xi_0,q)=0. \end{cases} \tag{28}$$

The solution of the MME [Eq. (23)] can also be contemplated as an independent eigenvalue problem, but now, q is the unknown eigenvalue and α is the fixed parameter. As above, we can express the eigenvalues associated to α and β as ${}_eq_m(\alpha)$ and ${}_oq_m(\beta)$, respectively, where $m\geq 1$ and the subindex e or o refers to even or odd MMF. The plots of ${}_eq_m(\alpha)$ and ${}_oq_m(\beta)$ are shown in Fig. 6. Since the solution $\varphi(\xi,\eta)$ is the product of solutions of Eqs. (23) and (24) for *the same value of* α (β) *and* q, then there exist a valid solution for each cross-point between the two families of curves. In other words, the MMF are decreasing-oscillatory non-periodic functions similarly to Bessel functions, therefore, if we choose a certain order r we have an infinite set of possible values of q that satisfy Eq. (28).

Let $q_{r,m}$ be the m-th zero of MMF of r-order. According to Eq. (25) for each $q_{r,m}$ there exist a corresponding energy eigenvalue $E_{r,m}$ associated to the eigenfunction $\varphi_{r,m}(\xi,\eta)$

$${}_eE_{r,m}=\left(\frac{2\hbar^2}{Mf^2}\right)q_{r,m}=\left(\frac{2\hbar^2}{Ma^2}\right)\frac{q_{r,m}}{e^2}, \tag{29}$$

where e is the eccentricity of the ellipse and a is the semi-major axis. The energy eigenvalues are proportional to $q_{r,m}$, therefore, the q-axis in Fig. 6 may be considered as an E-axis in $2\hbar^2/Mf^2$ units. The energy eigenvalues are the projections of the intersection-points on the E-axis.

The eigenvalues of the second constant of motion Λ can be directly obtained from Eq. (9) by substituting the momentum operators $p_\xi = -i\hbar\partial/\partial\xi$ and $p_\eta = -i\hbar\partial/\partial\eta$

$$\frac{f^2\hbar^2}{\hbar^2}\left(\sin^2\eta\frac{\partial^2}{\partial\xi^2} - \sinh^2\xi\frac{\partial^2}{\partial\eta^2}\right)\varphi = \Lambda\varphi.$$

By supposing the solution $\varphi(\xi,\eta) = R(\xi)\Theta(\eta)$, the above Equation is separated into two Mathieu equations [Eqs. (23) and (24)], where $\alpha = \Lambda/\hbar^2 - C/2$ and $q = -C/4$, and C is a constant of separation. It follows that the eigenvalue problem of Λ is equivalent to eigenvalue problem of H if Λ is chosen such that $\Lambda = (\alpha - 2q)\hbar^2$, where α and q are the eigenvalues of the hamiltonian problem. According to Eqs. (10) and (29), γ is given by

$$\gamma = \frac{\alpha - 2q}{4q}. \tag{30}$$

The separatrix $\gamma = 0$ is represented on the (α, q)-plane by the straight line $\alpha = 2q$, and it divides the plane into two zones, the rotating region $\gamma > 0$ and the oscillating region $\gamma < 0$ (see Fig. 6). The vertical distance between an intersection and the separatrix coincide with the value of Λ in $\hbar^2$ units. The classical limit for oscillating motion is given by $\alpha = -2q$ (*i.e.*, $\gamma = -1$) and it is plotted in Fig. 6 as well.

The energy eigenvalues of the first 22 stationary states corresponding to data of Fig. 6 (*i.e.*, $e = 0.5$) are listed in Table I, where we can see that ${}_oE_{r,m} > {}_eE_{r,m}$. The oscillating modes are always non-degenerate, whereas the rotating modes become more degenerate as γ increases.

In Fig. 7, we plot ${}_{e,o}E_{r,m}$ for ellipses with geometry from Figs. 2 and 4, (*i.e.*, $e = 0.5$ and $e = 0.924$ respectively) in increasing order. Since the energy depends on the focal distance [Eq. (29)], the eigenvalues must be scaled accordingly to make applicable comparisons. The even and odd eigenvalues are plotted separately in order to be aware of their different behavior. The straight lines connect ${}_eE_{r,1}$ with ${}_oE_{r,1}$, $(r = 1, 2, 3, \ldots)$ as a form to visualize the tendency ${}_eE_{r,m} \simeq {}_oE_{r,m}$ as r increases. This trend is more notorious as $e \to 0$ and, in the circular limit, (*i.e.*, $e = 0$) the eigenvalues satisfy ${}_eE_{r,m} = {}_oE_{r,m}$. This behavior can be appreciated also in the Fig. 6 where the square and circle markers get closer as the energy (*i.e.*, q value) increases.

TABLE I. Eigenvalues of energy (in $2\hbar^2/Ma^2$ units) and γ corresponding to first 22 stationary states.

State	E	(r,m)	γ	Motion	W
1	1.6858	${}_e0,1$	−0.5517	O	0.2394
2	3.9729	${}_e1,1$	−0.0332	O	0.0964
3	4.5843	${}_o1,1$	−0.5629	O	0.1040
4	7.2693	${}_e2,1$	0.1897	R	0.1477
5	7.6806	${}_o2,1$	−0.0186	O	0.0013
6	9.2967	${}_e0,2$	−0.7068	O	0.1595
7	11.4389	${}_e3,1$	0.3589	R	0.1318
8	11.6409	${}_o3,1$	0.2918	R	0.0507
9	13.7318	${}_e1,2$	−0.3202	O	0.1413
10	15.5806	${}_o1,2$	−0.7633	O	0.1462
11	16.3332	${}_e4,1$	0.5213	R	0.1091
12	16.4067	${}_o4,1$	0.5039	R	0.0812
13	19.3709	${}_e2,2$	−0.1198	O	0.1510
14	20.9897	${}_o2,2$	−0.4084	O	0.0858
15	21.9001	${}_e5,1$	0.6721	R	0.1009
16	21.9219	${}_o5,1$	0.6682	R	0.0933
17	23.5324	${}_e0,3$	−0.8052	O	0.1500
18	26.1874	${}_e3,2$	−0.0051	O	0.0507
19	27.4137	${}_o3,2$	−0.1720	O	0.0442
20	28.1425	${}_e6,1$	0.8050	R	0.1003
21	28.1482	${}_o6,1$	0.8042	R	0.0985
22	30.0605	${}_e1,3$	−0.5000	O	0.1034

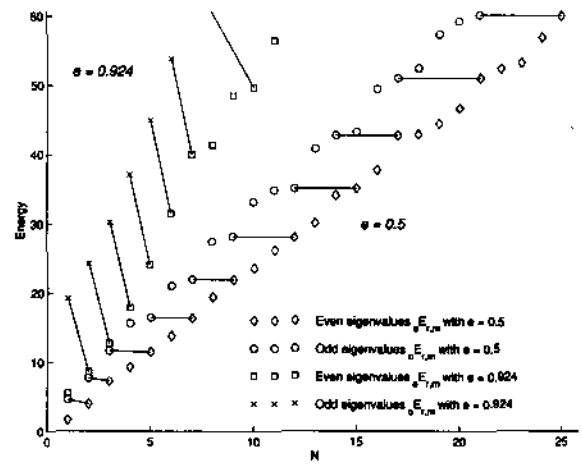

FIGURE 7. Increasing ordered energy eigenvalues (in $2\hbar^2/Ma^2$ units) for elliptic billiards with $e = 0.5$ and $e = 0.924$. We can appreciate that ${}_oE_{r,m} > {}_eE_{r,m}$, (see Table I).

4. Probability distributions

We first discuss the probability distributions in the quantum mechanics billiard. Excepting for the case $r = 0$, each eigenfunction $\varphi_{r,m}$ can be split into an even mode ${}_e\varphi_{r,m}$ and an odd mode ${}_o\varphi_{r,m}$. By using this notation, the eigenfunctions associated to $E_{r,m}$ in the elliptic quantum billiard are expressed in the following form

Even modes:

$${}_e\varphi_{r,m}(\xi,\eta) = Ce_r(\xi, {}_eq_{r,m})ce_r(\eta, {}_eq_{r,m}). \tag{31}$$

Odd modes:

$${}_o\varphi_{r,m}(\xi,\eta) = Se_r(\xi, {}_oq_{r,m})se_r(\eta, {}_oq_{r,m}). \tag{32}$$

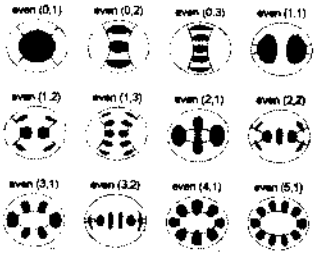

FIGURE 8. Probability distributions for the first even modes corresponding to data in Table I.

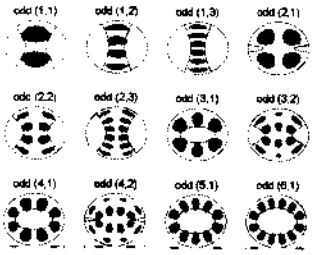

FIGURE 9. Probability distributions for the first odd modes corresponding to data in Table I.

In Figs. 8 and 9 we provide the probability densities $({}_{o,e}P_{r,m} = {}_{e,o}\varphi^2_{r,m})$ of the first even and odd modes from Table I. To compare with the classical solution, plots of the corresponding caustics are also included. The eccentricities of the caustics are related to γ (fourth column in Table I) by Eq. (11).

By observation of the probability distributions in Figs. 8 and 9 we can recognize that the mode $\varphi_{r,m}$ has r angular nodal-lines corresponding to $\eta =$ constant curves, and m radial nodal-lines corresponding to $\xi =$ constant curves including the boundary nodal-line.

The behavior of the radial density $R_{r,1}(\xi)$ as r increases is shown in Fig. 10a. The plots correspond to data from Table I, where we can observe that the first two modes $Ce_{0,1}$ and $Ce_{1,1}$ present oscillating motion. As r increases, the average value of the coordinate $\xi \to \xi_0$ and the motion became from oscillating to rotational kind. In Figs. 10b–10d, we compare the classical and quantum densities for motions with a very similar γ value. The classical distributions were obtained by dividing the whole range for ξ (or η) in 50 subdivisions and assuming the probability as proportional to the time spent by the particle in each subinterval. The vertical dashed line is the classical limit of motion. A bidimensional comparison between classical and quantum densities is given in Fig. 11.

In Figs. 8, 9, and 10 it is evident that quantum probability distributions penetrate the forbidden zone defined by the classical limit (*i.e.*, caustics). In order to quantify this penetration, we calculate the quotient

$$W = \frac{P_{\text{fz}}}{P_t} = \frac{\int_{\text{forbidden zone}} \left[\varphi_{r,m}(\xi,\eta)\right]^2 da}{\int_{\text{ellipse}} \left[\varphi_{r,m}(\xi,\eta)\right]^2 da},$$

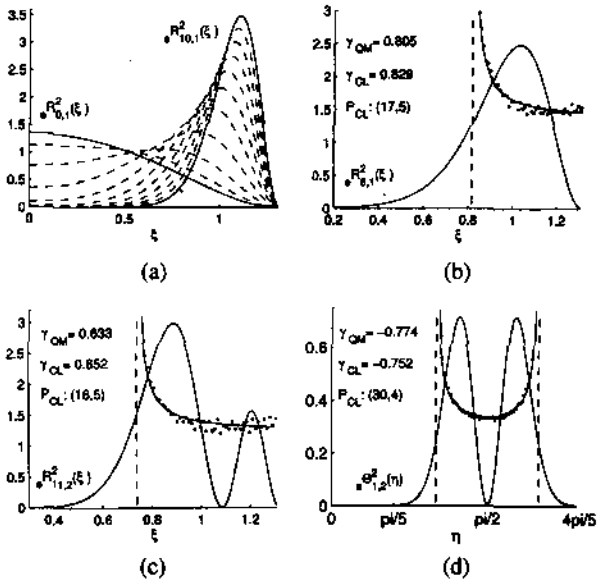

FIGURE 10. Comparison of quantum and classical probability densities. a) Transition of the radial probability $[\sim Ce^2_r({}_eq_{r,1},\xi)]$ from oscillatory motion to rotational motion. In b), c), and d) $P_{\text{CL}}: (r,n)$ is associated to a r-bounces classical trajectory.

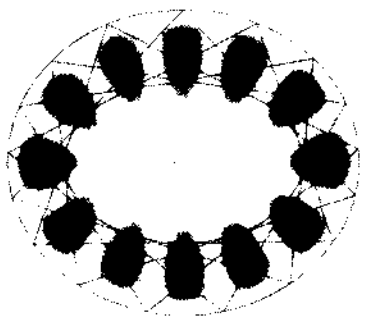

FIGURE 11. Probability distributions for the first odd modes corresponding to data in Table I.

where P_{fz} is the probability inside the forbidden classical zone, P_t is the probability in the whole ellipse, $da = h^2 d\xi d\eta = (f^2/2)(\cosh 2\xi - \cos 2\eta)$ is the differential element of area, and $\varphi_{r,m}(\xi,\eta)$ are the eigenfunctions given by Eqs. (31) and (32). After replacing the above expressions in W, we obtain for even modes

$$W = \frac{K \int_0^{\xi_c} \int_0^{\eta_c} Ce_r^2(\xi) ce_r^2(\eta)(\cosh 2\xi - \cos 2\eta)\, d\xi d\eta}{\int_0^{\xi_0} \int_0^{2\pi} Ce_r^2(\xi) ce_r^2(\eta)(\cosh 2\xi - \cos 2\eta)\, d\xi d\eta},$$

where the upper limits and the constant K depend on the forbidden zone (*i.e.*, on the sign of γ). For rotational motion ($\gamma > 0$), $\xi_c = \operatorname{arccosh}(1/e_c)$, $\eta_c = 2\pi$, and $K = 1$. For oscillating motion ($\gamma < 0$), $\xi_c = \xi_0$, $\eta_{\min} = \arccos(1/e_c)$, and $K = 4$. The double integrals in the above equation can be separated into one-dimensional integrals, the resulting expression is written as

$$W = K\frac{\int_0^{\xi_C} Ce_r^2\cosh(2\xi)\,d\xi\int_0^{\eta_C} ce_r^2\,d\eta - \int_0^{\xi_C} Ce_r^2\,d\xi\int_0^{\eta_C} ce_r^2\cos(2\eta)\,d\eta}{\pi\int_0^{\xi_0} Ce_r^2\cosh(2\xi)\,d\xi - \int_0^{\xi_0} Ce_r^2\,d\xi\int_0^{2\pi} ce_r^2\cos(2\eta)\,d\eta}, \tag{33}$$

where the orthogonality property $\int_0^{2\pi} ce_r^2\,d\eta = \pi$, has been used in the denominator. We apply a Newton-Cotes high-order method to evaluate the integrals in Eq. (33). The results for the first 22 modes are given in the sixth column of Table I.

4.1. Comparison with the circular billiard

In this subsection we compare the solutions of elliptic billiards with respect to known results of the circular billiards. The solution for the circular quantum billiard is well-known in the literature [3]. For a circular billiard of radius a, the degenerate eigenfunctions are given by

$$\varphi_{r,m}(\rho,\theta) = J_r(k_{r,m}\rho)\begin{pmatrix}\cos r\theta\\ \sin r\theta\end{pmatrix},$$

where J_r is the r-th order Bessel function, (ρ,θ) are the circular cylindrical coordinates, and $k_{r,m}$ is determined by satisfying the Dirichlet condition at boundary, $J_r(k_r a) = 0$. Then

$$q_{r,m} \equiv k_r a = a\sqrt{\frac{2ME_{r,m}}{\hbar^2}},$$

where $q_{r,m}$ is the m-th zero of the J_r Bessel function. Finally, the energy eigenvalues are given by

$$E_{r,m} = \left(\frac{2\hbar^2}{Ma^2}\right)\frac{q_{r,m}^2}{4}. \tag{34}$$

In Table II we compare the first eigenvalues of energy for a circular billiard of radius a, and for an elliptic billiard of major semi-axis a with $e = 0.2$ (*i.e.*, $b \simeq 0.98a$). According to Eqs. (29) and (34), the elliptic and circular energy eigenvalues are proportional to $q_{r,m}/e^2$ and $q_{r,m}^2/4$, respectively. Despite the axes of the ellipse still have very similar values, it is enough to show that each circular mode splits into an even mode and an odd mode. In Table II we can also see that the even modes have lower energy eigenvalues than odd modes. By comparing Table II with respect to Table I, it is notorious that decreasing the eccentricity implies a reduction in the corresponding energy eigenvalues.

TABLE II. Comparison of the eigenvalues of energy (in $2\hbar^2/Ma^2$ units) for a circular and an elliptic billiard.

State	Circular		Elliptic	
	E	(r,m)	E	(r,m)
1	1.4458	0, 1	1.4759	${}_e0,1$
2	3.6705	1, 1	3.7087	${}_e1,1$
3			3.7851	${}_o1,1$
4	6.5937	2, 1	6.7210	${}_e2,1$
5			6.7308	${}_o2,1$
6	7.6178	0, 2	7.7863	${}_e0,2$
7	10.1766	3, 1	10.3823	${}_e3,1$
8			10.3830	${}_o3,1$
9	12.3046	1, 2	12.4385	${}_e1,2$
10			12.6942	${}_o1,2$
11	14.3957	4, 1	14.6881	${}_e4,1$
12			14.6861	${}_o4,1$
13	17.7125	2, 2	18.0231	${}_e2,2$
14			18.0879	${}_o2,2$
15	18.7218	0, 3	19.1766	${}_e0,3$
16	19.2347	5, 1	19.6260	${}_e5,1$
17			19.6260	${}_o5,1$

5. Conclusions

We have compared the probability distributions of periodic trajectories inside a classical and a quantum elliptic billiard. The most important results are summarized as follows

i) The periodic trajectories in classical elliptic billiards are characterized by eigenvalues of equations involving elliptic integrals. There are two kinds of motion, corresponding to elliptic and hyperbolic caustics inside the billiard. The introduction of the parameter γ, Eq. (10), is appropriate because it allows us to make analogies between the classical and quantum case.

ii) By excepting the fundamental harmonics ($r = 0$), each eigenfunction $\varphi_{r,m}$ in the quantum elliptic billiard can be separated into an even eigenfunction ${}_e\varphi_{r,m}$ and an odd eigenfunction ${}_o\varphi_{r,m}$. This separation is irrelevant in a circular billiard.

iii) The odd energy eigenvalues are larger than even eigenvalues. The difference in energy increases with the eccentricity of the ellipse. In this manner, as $e \to 0$, both energy eigenvalues get closer and tend to the eigenvalue of the circular billiard, the motion becomes more rotational (elliptic caustics in the classical billiard). On the contrary, the γ values in even eigenfunctions are larger than odd eigenfunctions. The oscillating modes are always non-degenerate, whereas the rotating modes become more degenerate as γ increases.

The eigenfunctions in the elliptic quantum billiard can be expressed as alinear combination of Mathieu functions. We have shown graphically typical probability-patterns for different eccentricities of the elliptic boundary. The effect of ellipticity of the boundary has been found to be of great importance on the eigenfunction structure. We have also presented interesting differences between the circular and elliptical billiards.

Acknowledgments

The authors are grateful to Dr. Eugenio Ley Koo for constructive suggestions and discussions concerning the manuscript and Mathieu functions. This work was partially supported by CONACyT.

1. A. Yariv, *An Introduction to Theory and Applications of Quantum Mechanics*, (John Wiley & Sons, New York, 1982); A. Goswami, *Quantum Mechanics*, (Wm. C. Brown Publishers, London, 1992).
2. R.L. Liboff, *Introductory Quantum Mechanics*, (John Wiley & Sons, New York, 1992); C. Cohen-Tannoudji, B. Diu, and F. Laloë, *Quantum Mechanics*, (John Wiley & Sons, New York, 1977).
3. R.W. Robinett, *Am. J. Phys.* **64** (1996) 440.
4. M.F. Crommie, C.P. Lutz, and D.M. Eigler, *Science* **262** (1993) 218.
5. M.C. Gutzwiller, *Chaos in Classical and Quantum Mechanics*, (Springer-Verlag, New York, 1990).
6. Shau-Jin and R. Friedberg, *J. Math. Phys.* **29** (1988) 1537.
7. M. Sieber, *J. Phys. A* **30** (1997) 4563.
8. H. Waalkens, J. Wiersig, and H.R. Dullin, *Annals of Phys.* **260** (1997) 50.
9. R. van Zon and T.W. Ruijgrok, *Eur. J. Phys.* **19** (1998) 77.
10. J.C. Gutiérrez-Vega, S. Chávez-Cerda, and R.M. Rodríguez-Dagnino, *Rev. Mex. Fis.* **45** (1999) 613.
11. J.C. Gutiérrez-Vega, R.M. Rodríguez-Dagnino, and S. Chávez-Cerda, "Distribuciones de Probabilidad Clásicas y Cuánticas en Billares Elípticos", *XLII Congreso Nacional de Física, (7SB5)*, Noviembre de 1999, Villahermosa, Tab., México.
12. J. Zhang, A.C. Merchand, and W.D.M. Rae, *Eur. J. Phys.* **15** (1994) 133.
13. H. Goldstein, *Classical Mechanics*, second edition, (Addison-Wesley, Boston, 1980).
14. M. Abramowitz and I. Stegun, *Handbook of Mathematical Functions*, (Dover Inc., New York, 1964).
15. MatLab, Ver. 5.2, The Mathworks Inc. (1997).
16. N.W. McLachlan, *Theory and Application of Mathieu Functions*, (Oxford Press, United Kingdom, 1951).